Since January 2020 Elsevier has created a COVID-19 resource centre with free information in English and Mandarin on the novel coronavirus COVID-19. The COVID-19 resource centre is hosted on Elsevier Connect, the company's public news and information website.

Journal of Saudi Chemical Society (2022) **26**, 101473

King Saud University

Journal of Saudi Chemical Society

www.ksu.edu.sa
www.sciencedirect.com

ORIGINAL ARTICLE

In-silico investigation of phenolic compounds from leaves of *Phillyrea angustifolia* L. as a potential inhibitor against the SARS-CoV-2 main protease (M^{pro} PDB ID:5R83) using a virtual screening method

Ahmed Boufissiou [a], Mohnad Abdalla [b,*,1], Mohamed Sharaf [c,d], Saud I. Al-Resayes [e], Kadi Imededdine [f], Mahboob Alam [g,*], Sakina Yagi [h], Mohammad Azam [e,*], Mohamed Yousfi [a]

[a] *Laboratoire des Sciences Fondamentales (LSF), Université Amar Telidji de Laghouat, BP 37G, Route de Ghardaïa, 03000 Laghouat, Algeria*
[b] *Key Laboratory of Chemical Biology (Ministry of Education), Department of Pharmaceutics, School of Pharmaceutical Sciences, Cheeloo College of Medicine, Shandong University, 44 Cultural West Road, Shandong Province 250012, PR China*
[c] *Department of Biochemistry, Faculty of Agriculture, AL-Azhar University, Nasr City, Cairo 11651, Egypt*
[d] *Department of Biochemistry and Molecular Biology, College of Marine Life Sciences, Ocean University of China, Qingdao 266003, PR China*
[e] *Department of Chemistry, College of Science, King Saud University, P.O. Box 2455, Riyadh 11451, Saudi Arabia*
[f] *Centre National de Recherche en Biotechnologie (CRBt. 25000, Constantine), Algeria*
[g] *Department of Safety Engineering, Dongguk University, 123 Dongdae-ro, Gyeongju, Gyeongbuk 780714, South Korea*
[h] *Department of Botany, Faculty of Science, University of Khartoum, Sudan*

Received 16 February 2022; revised 29 March 2022; accepted 30 March 2022
Available online 6 April 2022

* Corresponding authors.
E-mail addresses: mohnadabdalla200@gmail.com (M. Abdalla), mahboobchem@gmail.com (M. Alam), azam_res@yahoo.com (M. Azam).
[1] This author equally contributed in the present work.
Peer review under responsibility of King Saud University.

Production and hosting by Elsevier

https://doi.org/10.1016/j.jscs.2022.101473

KEYWORDS

COVID-19;
Phillyrea angustifolia;
Phenolic compounds;
Molecular docking;
Molecular dynamics simulation

Abstract There is currently a global COVID-19 pandemic caused by the severe acute respiratory syndrome Coronavirus-2 (SARS-CoV-2) and its variants. This highly contagious viral disease continues to pose a major health threat global. The discovery of vaccinations is not enough to prevent their spread and dire consequences. To take advantage of the current drugs and isolated compounds, and immediately qualifying approach is required. The aim of our research is evaluation the potency for natural antiviral compounds against the SARS CoV-2 M^{pro}. Molecular docking of four phenolic compounds from *Phillyrea angustifolia* leaves with SARS-CoV-2 M^{pro} has been conducted. Similarly, the stability of selected ligand–protein interactions has been determined using MD simulations. Moreover, the quantitative structure–activity relationship (QSAR), MMGBSA binding energies, pharmacokinetics, and drug-likeness predictions for selected phenolic have been reported. The selected phenolic compounds (Luteolin-7-O-glucoside, Apigenin-7-O-glucoside, Demethyl-oleuropein, and Oleuropein aglycone) revealed strong binding contacts in the two active pockets of a target protein of SARS-CoV-2 M^{pro} with the docking scores and highest binding energies with a binding energy of −8.2 kcal/mol; −7.8 kcal/mol; −7.2 kcal/mol and −7.0 kcal/mol respectively. Both Demethyloleoeuropein and Oleuropein aglycone can interact with residues His41 and Cys145 (catalytic dyad) and other amino acids of the binding pocket of M^{pro}. According to QSAR, studies on pharmacokinetics and drug-like properties suggested that oleuropein aglycone could be the best inhibitor of SARS-CoV-2 for new drug design and development. Further *in vivo, in vitro,* and clinical studies are highly needed to examine the potential of these phenolic compounds in the fight against COVID-19.

1. Introduction

The story of the SARS-CoV-2 pandemic starts with a patient who was detected with evident signs of acute respiratory sickness on November 17, 2019. A month later, the number of new patients continued to rise, reaching five cases with comparable symptoms each day on average, all of whom were hospitalized in Wuhan Hospital, Hubei Region, for treating pneumonia, named by the World Health Organization as Coronavirus Disease 2019 (COVID-19). On January 7, 2020, after deep sequencing analysis, the Chinese authorities validated that it was certainly a novel virus of unknown origin from the coronavirus family "2019-nCoV" [1]. The most common symptoms are fever, cough, tiredness, and difficulty breathing. SARS-CoV-2 is believed to be most commonly spread by respiratory droplets that are produced when an infected patient speaks, coughs, or sneezes. The deaths are mainly due to the elderly. Fortunately, children were rarely affected without death. But the further course of this pandemic is unknown at this point [2]. The average incubation period ranges from 5 to 6 days, and the maximum range varies from 2 to 14 days [3]. According to the WHO status report, over 93 million reported cases and over 2 million deaths globally since the epidemic on January 17, 2021, 10 a.m. CET.

The main protease M^{pro} is one of the most targets for drug development against COVID-19. The M^{pro} is vital for virus production by the infected cell because it participates in the maturation, the interest in the search for inhibitors is of extreme importance as it inhibits the viral replication of SARS-CoV-2, making the M^{pro} an excellent drug target with great promise [4]. Although research is ongoing into various aspects of the nature and pathogenicity of the virus, a recent study has shown that mutations in the SARS-CoV-2 spike protein, by rearranging itself in response to changes in ACE2 or drugs targeting the protein region have created a barrier to develop a new drug against SARS-CoV-2, or effectively achieve a specific treatment [5–7].

As mentioned above, we can consider SARS-CoV-2 M^{pro} as the most interesting molecular target for the pharmacotherapy of COVID-19 due to its highly specific structure conserved substrate-binding region and a high degree of similarity in all members of the coronavirus's family such as SARS-CoV-2, SARS-CoV, and MERS-CoV. The degree of similarity and specific structure of M^{pro} can be used to develop new protease inhibitors [8,9]. Also, M^{pro} contains two catalytic domains, each containing six-stranded antiparallel β-barrel. In addition to vaccines, several efforts are being made to find potential drugs that inhibit viral main protease. A preliminary study has suggested the potential use of protease inhibitor lopinavir/ritonavir, commonly used drugs for the treatment of COVID-19 patients. Unfortunately, these drugs are not clinically acceptable. Additionally, several other viral protease inhibitors are under study for founding the treatment of SARS-CoV-2 infection [10].

In December 2021, the Food and Drug Administration (FDA) approved the emergency use authorization of the oral antiviral Paxlovid (nirmatrelvir/ritonavir) for the treatment of SARS-CoV-2 infection. In addition, Paxlovid consists of nirmatrelvir, which inhibits a SARS-CoV-2 M^{pro}, and a low dose of ritonavir, which slows down the metabolism of nirmatrelvir breakdown to help it remain in the body for a longer period at higher concentrations and helps in fighting the virus [11–13].

Based on ethnomedical studies, herbal medicines are used extensively in the treatment and prevention of several infectious diseases. A wide range of natural compounds identified in several plant species have shown antiviral activities, natural compounds such as phenolic compounds could be useful in the

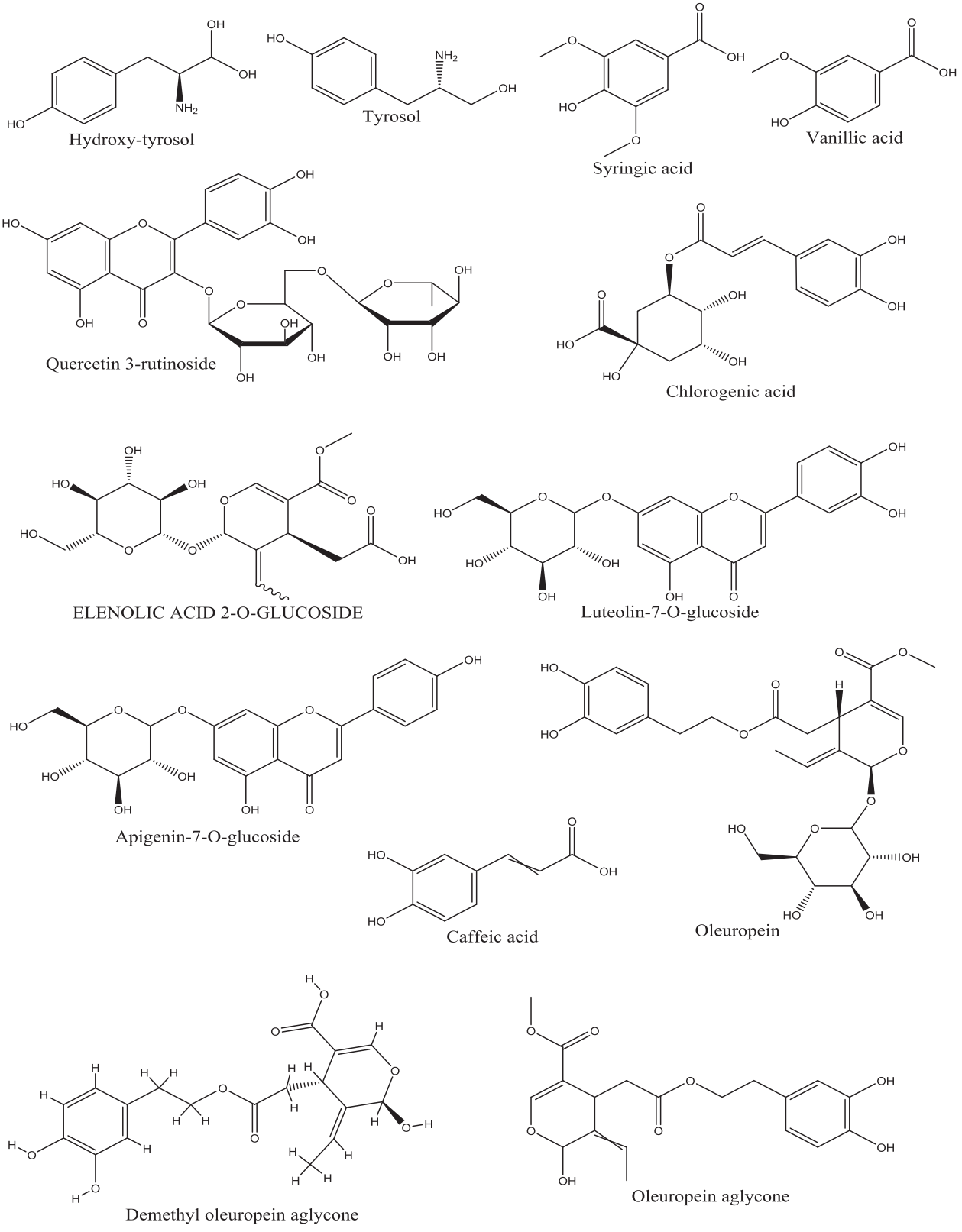

Fig. 1 The 13 phenolic compounds detected in the leaves of *Phillyrea angustifolia L.*

development of new anti-Covid-19 drugs [14–16]. More than 13 phenolic compounds have been identified in the leaves of *Phillyrea angustifolia* [17]. In the current research paper, we have evaluated *in-silico* the inhibitory potential of the previous 13 phenolic compounds (Fig. 1) against the crystal structure of the main protease M^{pro} (PDB ID:5R83). The *docking approach can predict the in-silico study of these phenolic compounds*. The four potential phenol compounds have been chosen in comparison with the native ligand (K0G) and according to their rank in the value of binding energy. In addition, MD simulations were performed to determine the stability of ligand–protein interactions. Also, quantitative structure–activity relationships (QSAR), MMGBSA binding energies, pharmacokinetics, and drug-likeness predictions were performed for selected phenolic compounds.

2. Materials and methods

2.1. Preparation of ligand

Through the exploitation of the PubChem online database (https://pubchem.ncbi.nlm.nih.gov/) [18], a two (3D)-dimensional structure of phenols compounds from leaves of *Phillyrea angustifolia* (Luteolin-7-O-glucoside, Apigenin-7-O-glucoside, Demethyl-oleuropein, and Oleuropein aglycone) used in the present study was obtained from PubChem. Moreover, geometrical optimization of these selected phenolic compounds was also carried out and saved in ".pdbqt" format using the MGLTools version 1.5.7.

2.2. Preparation of target

The 3D crystal structure of the M^{pro} protein (PDB ID:5R83 with resolution: 1.58 Å) was downloaded from the Protein Data Bank (PDB) (https://www.rcsb.org/) [19,20]. Crystallized with its native ligand (K0G), we used Discovery Studio Visualizer 2020 [21] to visualize the protein and delete all water molecules from the crystal structure of the M^{pro} protein. Empty atomic spaces and crystallographic perturbances were corrected by energy minimization with MGLTools version 1.5.7. Finally, the optimized protein structure was saved in pdbqt format.

2.3. QSAR studies

Quantitative structure–activity relationship (QSAR) is a method for discovering the relationship between structural properties of chemical substances and biological activity in a dataset of chemicals. Then, QSAR models predict the activities of new chemicals [22,23]. As a consequence of QSAR modeling, a large number of compounds may be selected based on their desired biological activities [24]. The purpose of the QSAR study is to support the results of molecular docking and to provide an expanded look at the chemical and pharmacological properties of selected phenolic compounds from leaves of *Phillyrea angustifolia*. The HyperChem Professional 8.0.3 application was used to do the computational calculations. The (MM +) force field and semi-empirical PM3 techniques were used to optimize all phenolic compounds, and the Fletcher-Reeves conjugate gradient algorithm was used to reduce the energy. *Log* P values have been used to assess the compound's biological activity and determine its permeability across cell membranes Other important properties such as mass, volume, surface area, total energy, free energy, hydration energy, refractive power, RMS gradient, and polarizability were calculated for all compounds [25].

2.4. Molecular docking study

A blind docking approach based on Autodock-Vina (version 4; The Scripps Research Institute, La Jolla, CA, USA) was used to determine the appropriate binding orientations of the ligands as well as the conformations with the targeted M^{pro} protein PDB ID 5R83. The docking of ligands is performed to the whole surface of a protein PDB ID 5R83 without prior determination of the target pocket. This is needed to calculate the preferred orientations of the ligand with the highest binding affinities for the protein active sites associated with structural pockets and cavities. After molecular docking, the binding of the four ligands with the specific amino acid residues has been visualized in Discovery Studio Visualizer 2020. The best poses were chosen based on the minimum binding energy required for the binding ligand to the protein. It should be noted that the protein–ligand docking protocol is Rigid receptor docking. During the docking process, the protein was fixed while the ligands were flexible.

2.5. Molecular dynamics (MD) simulation

The molecular dynamics simulation was carried out using the Desmond software package. The MD simulation software was used to assess the stability of the protein–ligand complexes. The OPLS 2005 force field and the Gromos9643a1 have been applied. Using Desmonds' system builder tool, the entire protein–ligand system in the cubic box in a cubic water box was solvated by the TIP3P water model in x, y, and z dimensions while maintaining a 12 Å buffer space. The system was neutralized with counterions of 0.15 M NaCl. The cubic water box Simple Point Charge (SPC) was applied. The system was neutralized with counterions of 0.15 M NaCl. The Simple Point Charge (SPC) cubic water box was applied. Energy minimization (50,000 ps) in two steps (NVT and NPT) was continued until the minimization was complete. The ambient pressure was set at 1.013 bar at a temperature of 310 K for 100 ns. The thermodynamic stability of wild-type (WT) and mutant (MT) E proteins was investigated using root mean square fluctuations (RMSF) and root mean square deviation (RMSD) (RMSD). To confirm and improve the results, the simulation was run three times. Each simulation was executed at about 1000 frames [16].

2.6. Binding free energy calculation

The Molecular Mechanics Generalized Born Surface Area (MMGBSA) method was applied to calculate the free energy of the binding of ligands to protein. The Prime module of Schrodinger estimated the binding free energy. The binding free energy between the protein SARS-CoV-2S M^{pro} and the Ligands was predicted using the MM-GBSA method at the last 20 ns time.

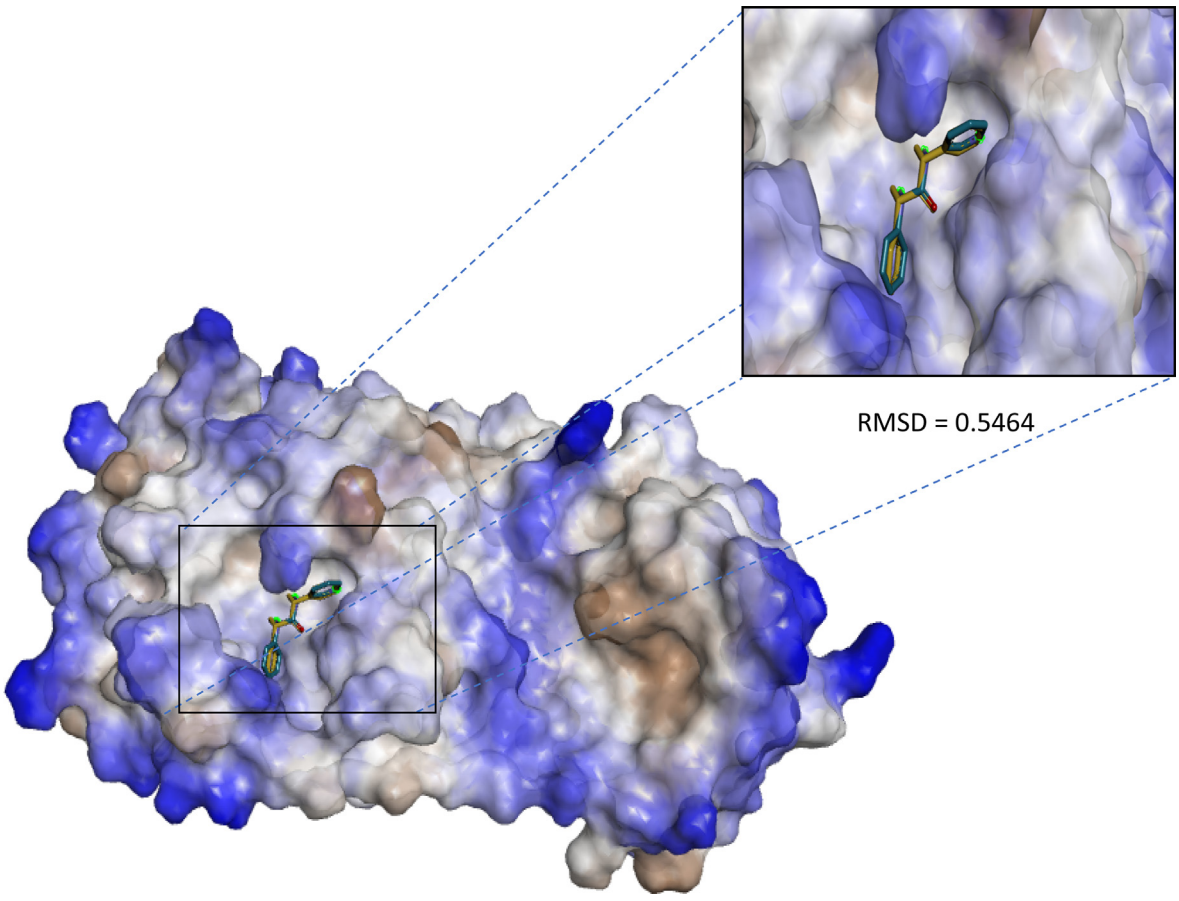

Fig. 2 The superimposition of KOG404 between the docking pose in green and the coordinated pose in yellow.

Table 1 QSAR data for the selected compounds.

Function	Luteolin-7-o-glucoside	Apigenin-7-o-glucoside	Demethyloleoeuropein	Oleuropein aglycone
Surface area (Approx) (Å^2)	640.75	623.99	776.04	535.82
Surface area (Grid) (Å^2)	632.95	585.97	781.67	526.36
Volume (Å^3)	1068.73	1023.43	1321.86	933.96
Hydration energy (Kcal/mole)	−42.67	−35.31	−41.12	−20.44
Log P	4.12	4.12	5.89	5.07
Refractivity (Å^3)	52.39	54.40	63.21	49.18
Polarizability (Å^3)	37.56	36.46	40.49	28.55
Mass (amu)	435.28	418.27	514.31	359.23
Total energy (kcal/mol)	9.09332	7.34232	10.8557	5.43942
Dipole Moment (Debye)	1.218	0.8316	1.1	1.106
RMS Gradient (kcal/ Å mol)	0.09384	0.09706	0.09499	0.09287

2.7. Pharmacokinetic and drug-likeness predictions

ADMET (Absorption, Distribution, Metabolism, Excretion, and Toxicity) studies have recently received much attention in computer-based drug development, they are used to identify the pharmacological structure. In the following steps, the Admits were assessed to predict the physicochemical properties of the selected phenolic compounds by using the website (https://www.swissadme.ch) [26], and the pharmacophoric properties were realized by pkCSM servers (https://biosig.unimelb.edu.au/pkcsm/) [27].

3. Results and discussion

3.1. Validation of the docking protocol

The docking protocol was confirmed by redocking the native ligand (KOG) from the 3D crystal structure of the Mpro pro-

tein (PDB ID:5R83) into the same binding pocket. The obtained binding affinity was −6.1 kcal/mol, Fig. 2 shows that the value of RMSD for two conformations is 0.5464 (Å), it is calculated by Discovery Studio 2020; which confirms that the used docking protocol is accurate because the RMSD value was less than 2.0 (Å) [28].

3.2. QSAR studies

QSAR shows some molecular descriptors of QSAR properties of the selected phenolic compounds. The presented values include *log* Surface area, Volume, Hydration energy, Refractivity, Polarizability, Mass, total energy, Dipole Moment, and RMS Gradient. The value of *log* P for Demethyloleoeuropein and Oleuropein aglycone was superior to the rest of the compounds. *Log* P is used to assess a compound biological activity as well as its permeability through cell membranes [29]. A high *log* P value means the molecule is hydrophobic, whereas a low value of *log* P indicates that the molecule is hydrophilic [30]. The calculated log P value of Demethyloleoeuropein and Oleuropein aglycone was bigger than the rest of the phenolic compounds. This means that the Demethyloleoeuropein and Oleuropein aglycone molecules are more hydrophilic and soluble than the Luteolin-7-O-glucoside and Apigenin-7-O-glucoside molecules, respectively as demonstrated in (Table1).

3.3. Molecular docking analysis

The current study of phenolic compounds suggests a promising efficacy against the SARS-CoV-2 [31,32]. The four phenolic compounds can also interact with the amino acids present in the binding pocket of M^{pro} inhibiting the synthesis of several proteins, which are required for the correct viral replication [33]. The binding interactions between the protein SARS-CoV-2S M^{pro} (PDB ID:5R83) and the four phenols compounds from leaves of *Phillyrea angustifolia* L were predicted using molecular docking. The three-dimensional crystal structure of M^{pro} is used as a target for the docking analysis. The interactions between the amino acids of the main protease (M^{pro}) and these phenolic compounds have also been identified Cys145, Thr26, Glu166, Thr25, Thr24, Met165, Asn142, Leu287, and Thr199. The 3D globular structural analysis revealed that the main protease (M^{pro}) form two binding pockets: binding pocket-1 at Cys145, Thr26, Glu166, Thr25, Thr24, Met165, and Asn142, the second-binding pocket-2at two amino acid residues Leu287 and Thr199 (Table 2).

The assayed docking scores for each phenolic compound that interacts with the major protease (M^{pro}) are shown in Fig. 3, Fig. 4, and Table 2, respectively. The binding energy values of the selected compounds range from −7.0 to −8.2, with Luteolin-7-O-glucoside having the greatest binding energy values. Apigenin-7-O-glucoside formed two H-bonds with polar amino acids (Thr199) and nonpolar amino acids (Leu287), two H-bonds due to the H-bond donor group and one due to the H-bond acceptor site existing in the ligand. Furthermore, Demethyloleoeuropein is shown five H-bonds with four polar amino acids (Thr26, Glu166, THR25) and nonpolar amino acids (Cys145). Additionally, Luteolin-7-O-glucoside reveals six H-bond interactions with four polar amino acids (Thr25, Thr24, Met165) and nonpolar amino acids (Cys145). Finally, Oleuropein aglycone shows interactions like a Demethyloleoeuropein, and additionally, it shows five H-bond interactions with two polar amino acids (Thr26, Asn142) and nonpolar amino acid (Cys145) (Table 3), interactions with key amino acid residues of M^{pro} (Cys145) were shown for almost all compounds. These findings indicated that all of the phenolic compounds under investigation have strong interactions with M^{pro}, with Luteolin-7-o-glucoside having the strongest capability (Table 3) to combat SARS-CoV-2S and hence might be used as a retargeted therapeutic drug for COVID-19.

3.4. Molecular dynamics simulation

To assess the conformational stability and fluctuation analysis of the protein–ligand complexes, a 100 ns molecular dynamics simulation was performed. The overall stability was investigated further using RMSD and RMSF analysis.

3.4.1. Stability profile analysis by root mean square deviation (RMSD)

The stability of the selected phenolic compounds within the two binding pockets (active site) of protein M^{pro} was investigated using MD simulation for 100 ns, the RMSD values of the protein–ligand complexes trajectories were calculated (Fig. 5). The RMSD analysis for the 5R83-Demethyloleoeuropein complex showed that the protein Cα-RMSD of 5R83-Demethyloleoeuropein reached stability within 05 ns and the results are shown in (Fig. 5C), in 5R83-Demethyloleoeuropein complex, the RMSD of Demethyloleoeuropein achieved stability nearby 05 ns and sustained up to 60 ns and then came to an equilibrium reaching 6 Å. Following then, the RMSD of compound Demethyloleoeuropein became unstable and run away from the active site as indicated by the remarkably high RMSD and trajectory analysis (Fig. 5C). Also, we found that the values of protein Cα-RMSD of 5R83-Luteolin-7-o-glucoside and 5R83-Oleuropein aglycone complexes are almost similar with protein Cα-RMSD of 5R83-Demethyloleoeuropein due to their ligands interact in the same pocket-1. In the same way, Oleuropein

Table 2 Molecular docking analysis and amino acid interaction of selected phenolic compounds.

Compound	Binding affinity (kcal/mol)	Torsional	Residues found in the active site	Num of H-bond	involve residues
Apigenin-7-o-glucoside	−7.8	10	LEU 287 and THR 199	2	LEU 287, THR 199
Demethyloleoeuropein	−7.2	17	CYS 145, THR 26, GLU 166,	5	CYS 145, THR 26, GLU 166, THR 25
Luteolin-7-o-glucoside	−8.2	11	THR 25, THR 24, MET 165,	6	CYS 145, THR 25, THR 24, MET 165
Oleuropein aglycone	−7.0	11	and ASN 142	5	CYS 145, THR 26, ASN 142

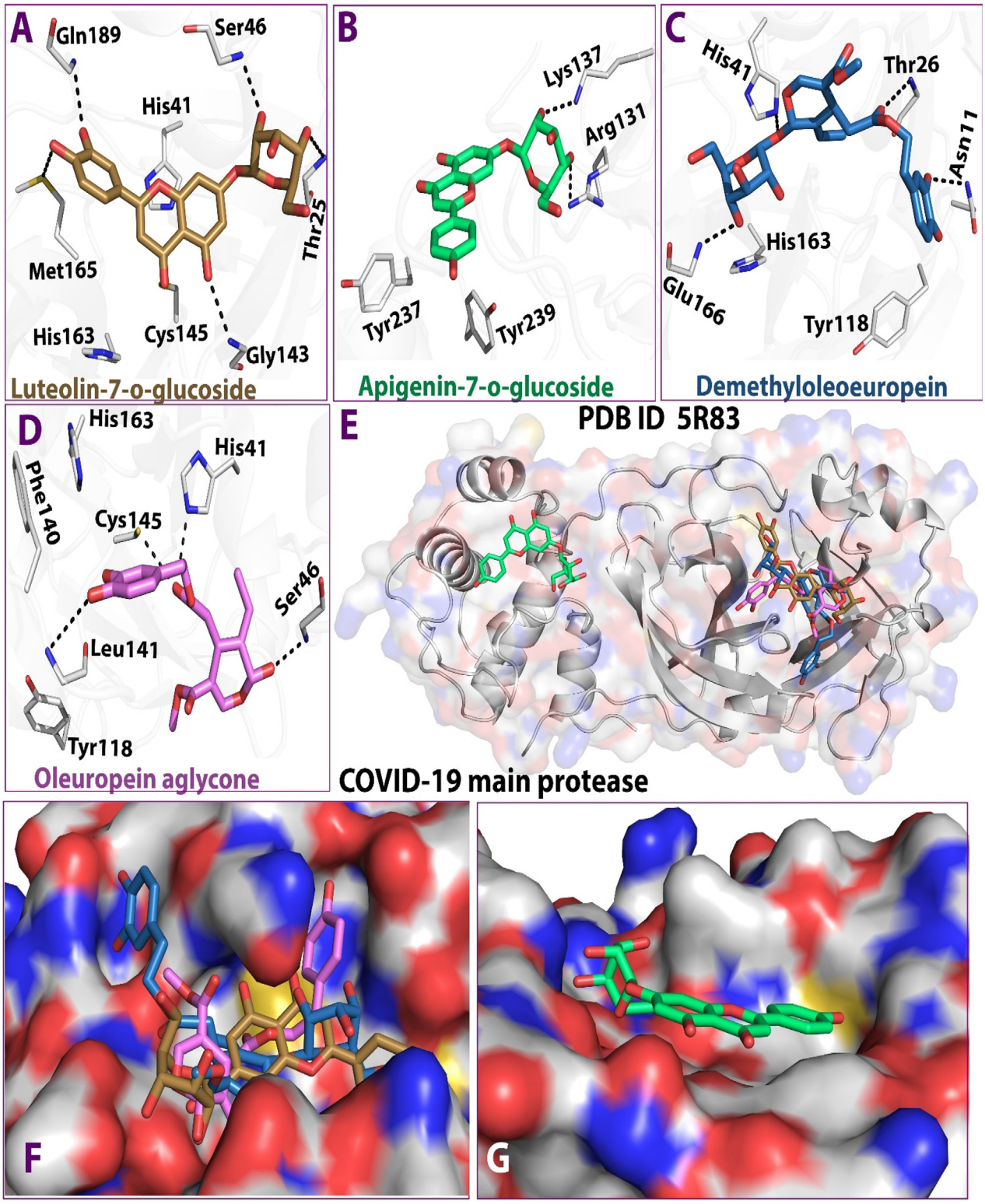

Fig. 3 3D ligand-receptor interactions of selected phenolic compounds with SARS-CoV-2 (M^{pro}).

aglycone RMSD of 5R83-Oleuropein aglycone complex showed initial fluctuations then achieved stability near 50 ns. After that, the RMSD of Oleuropein aglycone became stable, with fluctuations limited to a range of 6 mm (Fig. 5D). It can also be observed that Luteolin-7-o-glucoside (Fig. 5A) RMSD reveals initial fluctuations, then attained a maximum RMSD value of 25 Å at 20.0 ns and became stable and continued up to 80 ns after the RMSD of compound A became unstable. On the other hand, the protein Cα-RMSD of the 5R83-Apigenin-7-O-glucoside complex showed fluctuations between

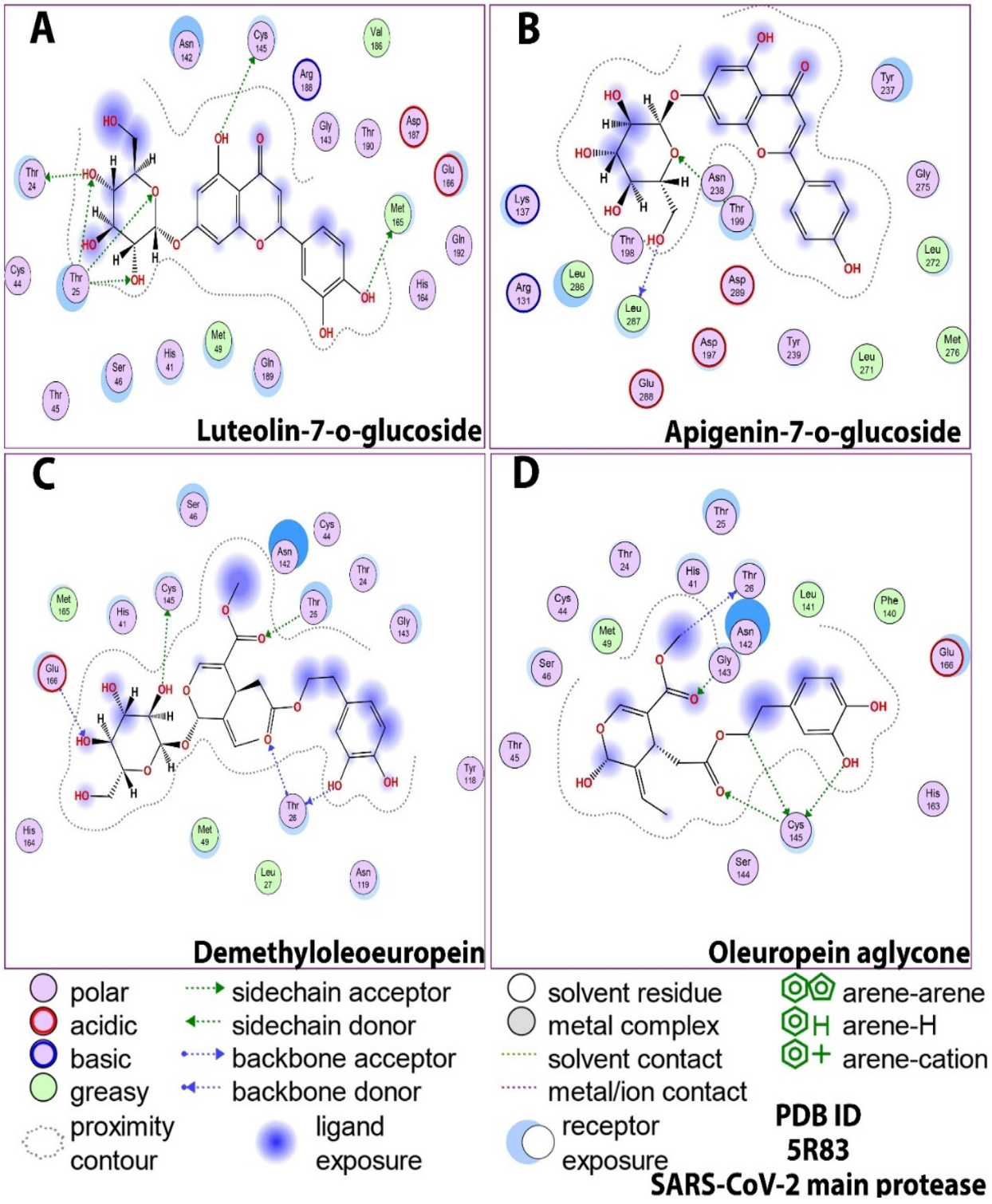

Fig. 4 2D ligand-receptor interaction of selected phenolic compounds with SARS-CoV-2 (M^{pro}).

5 and 40 ns, the RMSD fluctuations are between 1.8 and 2.1 Å, after 40 ns till the end of the simulation the range of fluctuations became narrow and stable at about 2.1 Å. It must be noted that Apigenin-7-O-glucoside interacted in the pocket-2, Apigenin-7-O-glucoside RMSD of 5R83-Apigenin-7-O-glucoside complex (Fig. 5B) showed instability value compared to other phenolic compounds, and it can be categorized to a three-time point early stage of the simulation 0–10 ns process around 5 Å, the second time points 10–55 ns got RMSD range 5–64 Å, At the third point in time, between 55 ns to the end of

Table 3 Binding energies (MMGBSA) of the complexes M^{pro} (5R83) and the selected phenolic compound.

Compound name	MMGBSA dG Bind (Kcal/mol)	MMGBSA dG Bind Coulomb (Kcal/mol)	MMGBSA dG Bind Covalent (Kcal/mol)	MMGBSA dG Bind Hbond (Kcal/mol)	MMGBSA dG Bind Lipo (Kcal/mol)	MMGBSA dG Bind Solv GB (Kcal/mol)	MMGBSA dG Bind vdW (Kcal/mol)
Apigenin-7-o-glucoside	−14,38	−0,14	0,24	−0,01	−4,46	3,67	−14,38
Demethyloleoeuropein	0,42	−0,84	0,01	0,00	1,54	−0,30	0,42
Luteolin-7-o-glucoside	−22,78	−16,57	2,54	−1,39	−6,88	19,66	−22,78
Oleuropein aglycone	−48,29	−37,65	3,22	−3,74	−10,29	30,99	−48,29

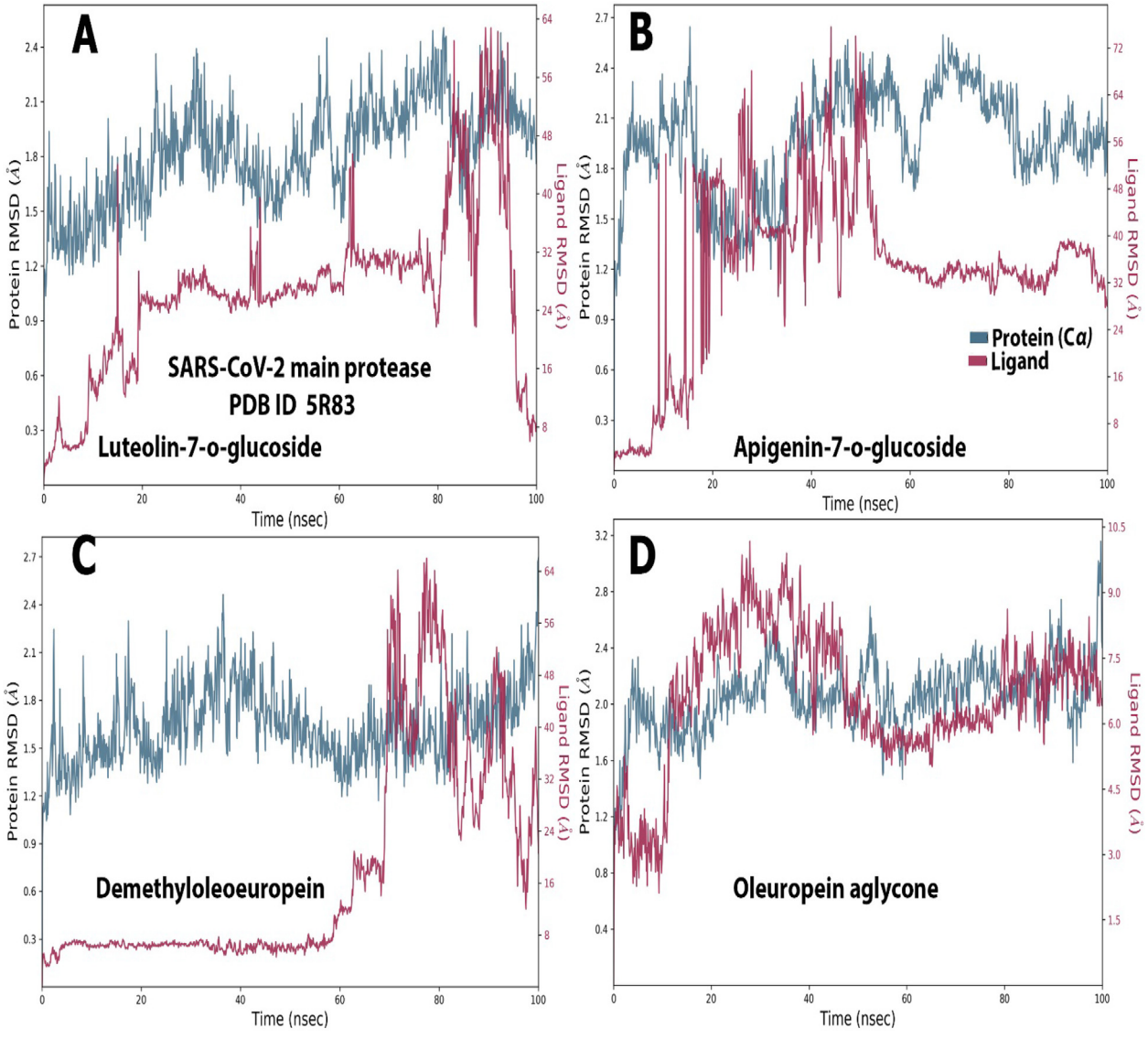

Fig. 5 RMSD plot obtained for (5R83-Luteolin-7-O-glucoside, 5R83-Apigenin-7-O-glucoside, 5R83-Demethyloleoeuropein and 5R83-Oleuropein aglycone) complexes: protein Cα and compound RMSD showed in blue and red color, respectively.

the simulation, the value of RMSD is gradually increased from 64 to 32 until it became stable, indicating equilibration of the geometry. In contrast, Luteolin-7-o-glucoside forms more H-bonding interactions with the binding pocket of 5R83 protein, while Apigenin-7-o-glucoside forms fewer number of H-bonds.

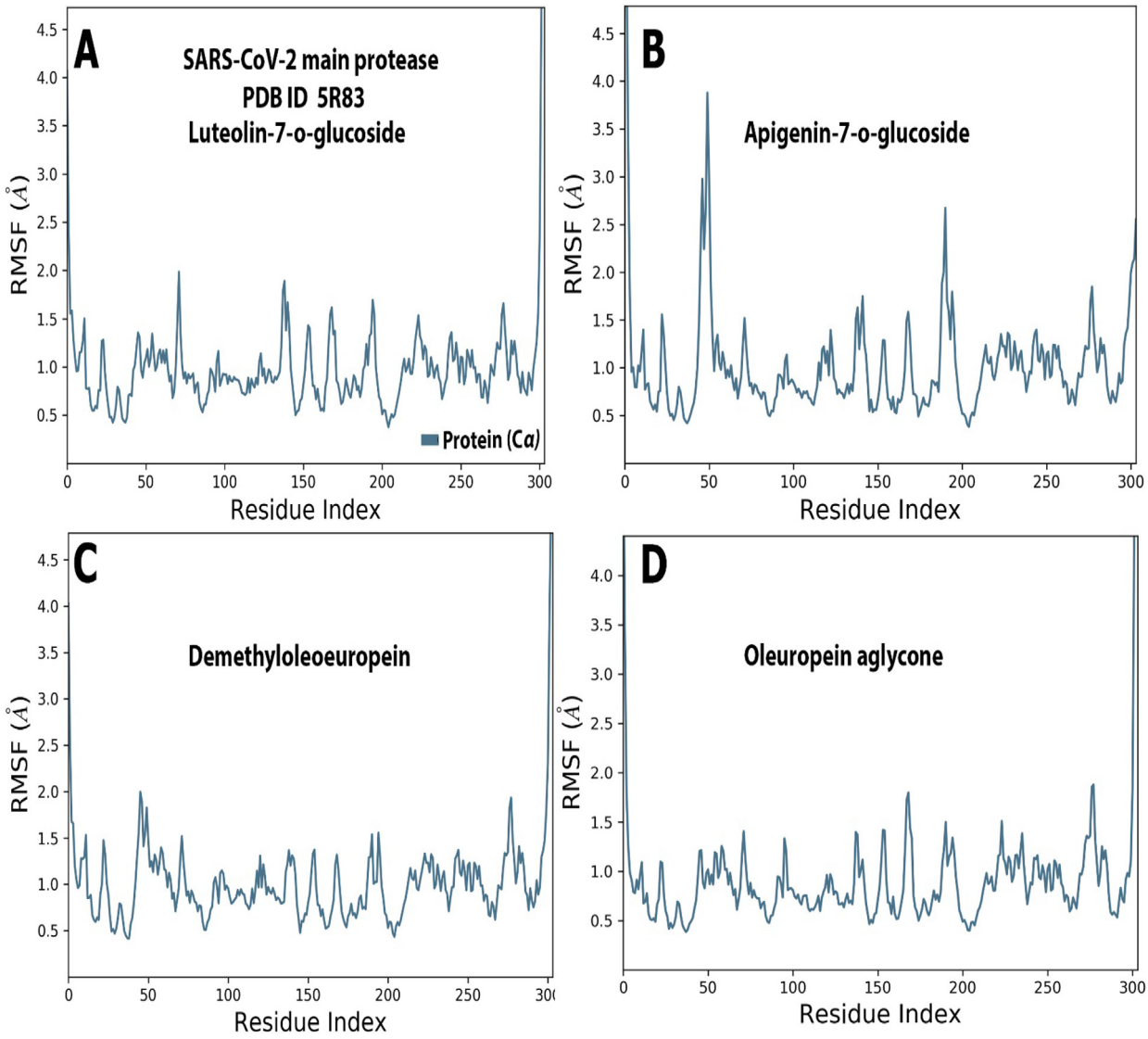

Fig. 6 RMSF plot obtained for (5R83-Luteolin-7-O-glucoside, 5R83-Apigenin-7-O-glucoside, 5R83-Demethyloleoeuropein, and 5R83-Oleuropein aglycone) complexes.

3.4.2. Stability profile analysis by root mean square fluctuation (RMSF)

About 306 residues of 5R83 were calculated using the root mean square fluctuation (RMSF) to explore the flexibility of every residue and the fluctuation of the residue during a simulation period. The RMSF of 5R83-Luteolin-7-O-glucoside, 5R83-Demethyloleoeuropein and 5R83-Oleuropein aglycone complexes are almost similar and all of them stayed less than 2 Å during the simulation. In comparison with the RMSF of 5R83-Apigenin-7-O-glucoside complex that revealed a local fluctuation for the whole sequence, it had two peaks fluctuation at (45–55) and at (190–200) residues (Fig. 6D). The two peak fluctuations were shown in binding pocket-2 of the M^{pro}, which validated the close interaction of Apigenin-7-O-glucoside to the binding pocket- 2 of M^{pro}. The maximum fluctuation of RMSF for the 5R83-Apigenin-7-O-glucoside complex was observed in the residue SER 46, ASP48, ASN 51, sn53, Asp58, Gly251, and Ala191 because they have high flexibility probably due to the proton side-chain and backbone φ and ψ angles responsible for the degree of rotation (Fig. 6) [34]. The wide-ranging fluctuations in RMSF and RMSD are indicating of system perturbance that could be caused by conformational changes within the protein complex system or ligand showing greater displacements inside binding sites. This has a significant impact on the complex-binding energies.

3.4.3. Ligand properties

Five properties have been investigated to illustrate the stability of the selected phenolic compounds in the two binding pockets of protein M^{pro} through the simulation of 100 ns, as revealed in Fig. 7. The ligand property was analyzed by calculating the ligand RMSD, molecular surface area (MolSA), accessible surface area (SASA), the radius of gyration (rGyr), solvent, and polar surface area (PSA). The RMSD of Luteolin-7-o-glucoside and Demethyloleoeuropein initially fluctuated up to 5 ns for 5R83-Luteolin-7-O-glucoside and 5R83-

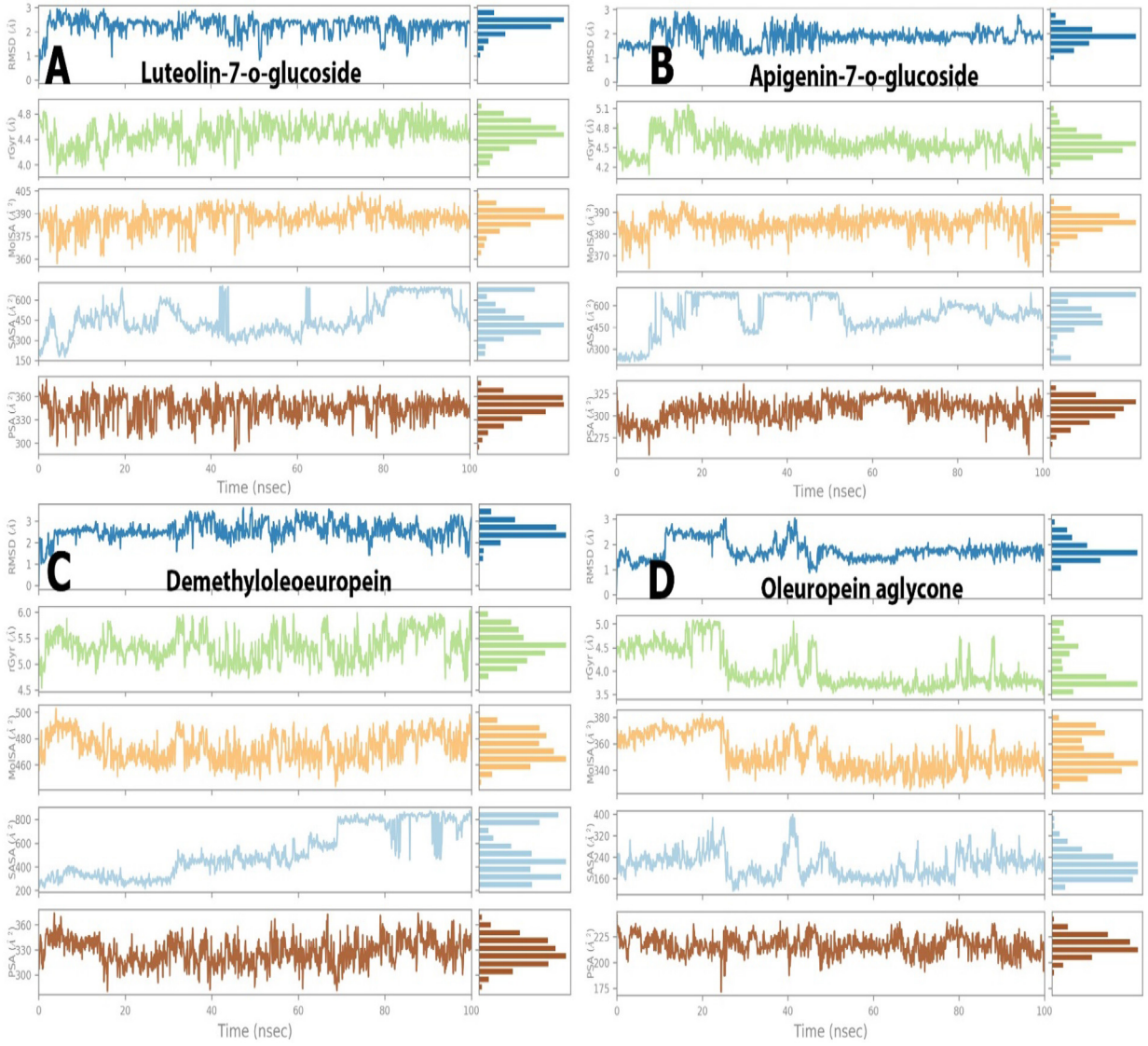

Fig. 7 Ligand property trajectory of the (5R83-Luteolin-7-O-glucoside, 5R83-Apigenin-7-O-glucoside, 5R83-Demethyloleoeuropein, and 5R83-Oleuropein aglycone) complexes.

Demethyloleoeuropein, and then gradually steadied for the rest of the MD simulation. The RMSD of Apigenin-7-O-glucoside and Oleuropein aglycone for 5R83-Apigenin-7-O-glucoside and 5R83-Oleuropein aglycone respectively had fluctuations in the beginning then gradually reached equilibrium at 10 ns of the simulation. The four phenolic compounds have shown a value of RMSD ranging from 1 to 3 Å and the equilibrium around 2.5 Å.

The MolSA values of selected phenolic compounds exhibited slight fluctuation ranging from around 340 to 390 $Å^2$ with equilibrium at 490 Å for Luteolin-7-o-glucoside andApigenin-7-O-glucoside, the Demethyloleoeuropein has been noticed in a range of 470 $Å^2$ to 490 $Å^2$ during most of the simulation time, the rest of Oleuropein aglycone showed the least fluctuations ranging from around 340 $Å^2$ to 370 $Å^2$ with equilibrium at 350 Å during the simulation.

The SASA values of four ligands started with a heavy fluctuation up to 50 ns simulation and then gradually converged to equilibrium. Except for Oleuropein aglycone, all the rest ligands (phenolic compounds) showed SASA values ranging from 200 $Å^2$ to 600 $Å^2$ with an equilibrium around 300 $Å^2$. Furthermore, the Oleuropein aglycone expressed fluctuations starting from 200 $Å^2$ and ending at 350 $Å^2$ during 50 ns but it was then found constant at 200 $Å^2$ throughout 100 ns with the least fluctuations.

Similarly, except for Oleuropein aglycone, the PSA of the rest ligands began with slight fluctuation but afterward reached the equilibrium state, these ligands are showing values of PSA range from 250 $Å^2$ to 360 $Å^2$ and the equilibrium around 340 $Å^2$. The lowest fluctuation of values of PSA was observed in Oleuropein aglycone, which ranges from 210 $Å^2$

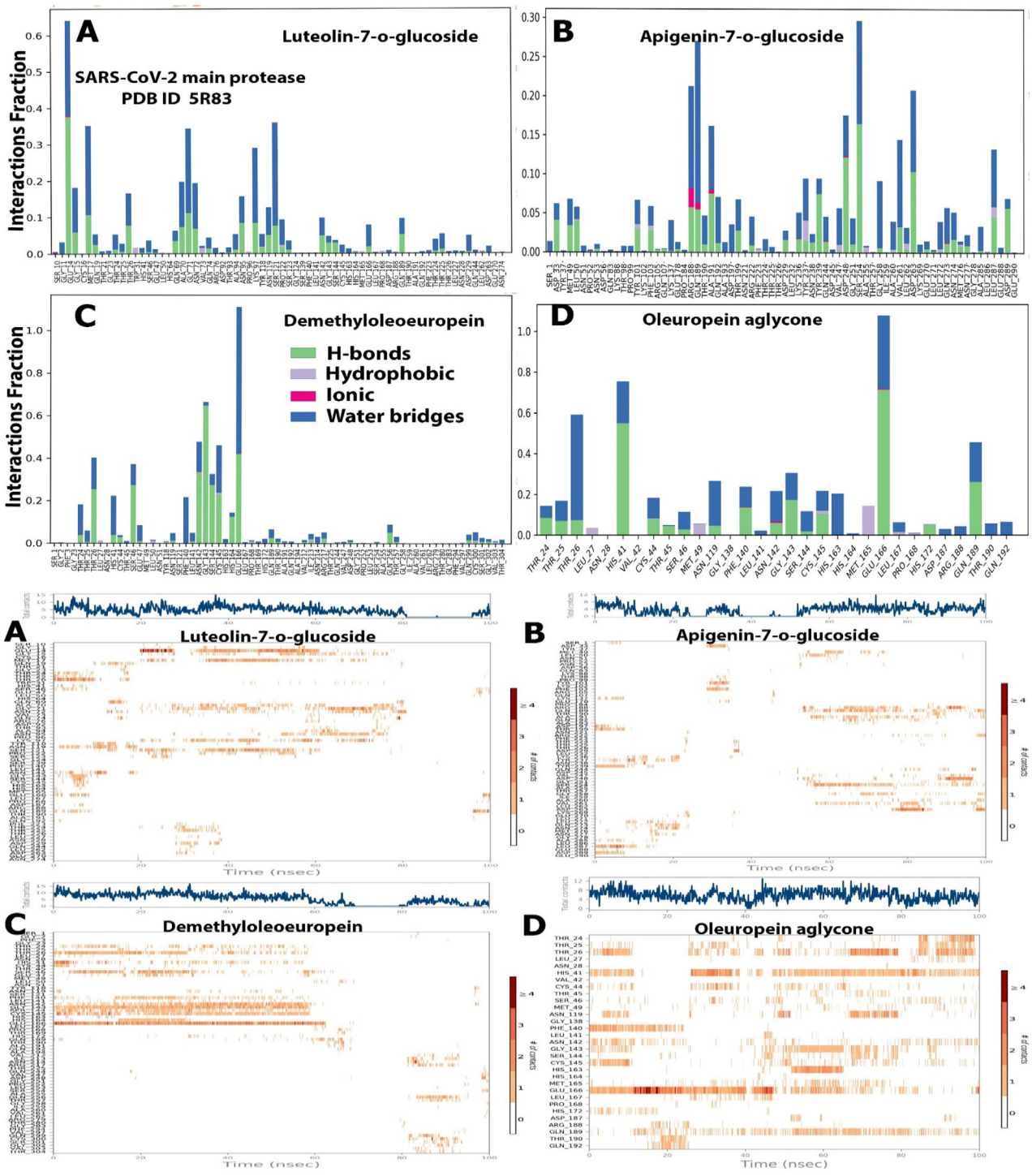

Fig. 8 Protein-ligand contact plots and interaction residues for the (5R83-Luteolin-7-O-glucoside, 5R83-Apigenin-7-O-glucoside, 5R83-Demethyloleoeuropein, and 5R83-Oleuropein aglycone) complexes.

to 230 Å^2 then attained a maximum PSA value of 225 Å at 5 ns and further got stable for the rest of the simulation time.

3.4.4. Protein–ligand contacts

Protein–ligand contacts provided the best understanding of the simulation and played an important role in drug development. They are divided into four types: hydrogen bonds, hydrophobic, ionic, and water bridges [35]. Hydrogen bonding (H-bonds) are playing an important role in protein–ligand interactions and protein folding [36]. Fig. 8 shows the active site amino acids histogram for 5R83-Apigenin-7-O-glucoside (mainly Asp33, Met49, Leu50, Tyr101, Phe103, Arg188, Gln189, Thr190, Ala191, Gln192, Thr199, Arg222, Asp229, Lys236, Thr237, Asn238, Tyr239, Gln244, Asp248, Gly251, Ser254, Gly258, Val261, Leu262, Asp263, Glu270, Gln273, Asn274, Met276, Asn277, Leu278, and Asp289) interacting

Table 4 *In-silico* physicochemical properties, medicinal chemistry profile, drug-likeness, absorption, and toxicity of selected phenolic compounds from leaves of *Phillyrea angustifolia* L.

Properties	Apigenin 7-glucoside	Demethyloleoeuropein	Luteolin-7-O-glucoside	Oleuropein aglycone
Physicochemical Properties				
Molecular weight	432.38 g/mol	526.49 g/mol	448.38 g/mol	378.37 g/mol
Consensus Log Po/w	0.55	−0.33	0.16	1.57
Num. rotatable bonds	4	10	4	8
Num. H-bond acceptors	10	13	11	8
Num. H-bond donors	6	7	7	3
TPSA	170.05 $Å^2$	212.67 $Å^2$	190.28 $Å^2$	122.52 $Å^2$
Drug likeness				
Lipinski	Yes; 1 violation: NHorOH > 5	No; 3 violations: MW > 500, NorO > 10, NHorOH > 5	No; 2 violations: NorO > 10, NHorOH > 5	Yes; 0 violation
Bioavailability Score	0.55	0.11	0.17	0.56
Medicinal Chemistry				
Lead likeness	No; 1 violation: MW > 350	No; 2 violations: MW > 350, Rotors > 7	No; 1 violation: MW > 350	No; 2 violations: MW > 350, Rotors > 7
Synthetic accessibility	5.12	6.12	5.17	4.63
Absorption				
Intestinal absorption (human)	37.609 (% Absorbed)	19.044 (% Absorbed)	37.556 (% Absorbed)	74.397 (% Absorbed)
Caco2 permeability (log Papp in 10–6 cm/s)	0.33	−0.834	0.248	0.61
Toxicity				
AMES toxicity	No	No	No	No
Max. tolerated dose (human)	0.515 (log mg/kg/day)	0.522 (log mg/kg/day)	0.584 (log mg/kg/day)	−0.505 (log mg/kg/day)
Hepatotoxicity	No	No	No	Yes
Skin Sensitization	No	No	No	No

through hydrogen bonds, where the ligands are indicated in Fig. 8. Arg188, Gln189, Ala191, Asp248, Ser254, Asp263 were among the most important residues that were proven to play a significant influence in ligand binding. The hydrophobic contacts for 5R83-Apigenin-7-O-glucoside are have been developed by the residues Tyr101, Phe103, Tyr237, Val247, Ala255, and Leu262. Moreover, 5R83-B water bridges have been found in the majority of residues along with hydrogen bonding. The residues Arg188, Gln189, Ala191, Lys236, Gln244, Asp248, Gln273 for 5R83-Apigenin-7-O-glucoside have shown some ionic interactions with the Apigenin-7-O-glucoside.

The amino acids (mainly Glu14, Gly15, Mrt17, Gln19, Thr24, Thr26, Gln69, Ala70, Gly71, Asn72, Gln74, Asn95, Lys97, Try118, Asn119, Ser121, Pro122, Ser123, Asn142, Gly143, Ser144, and Glu189 for 5R83-Luteolin-7-O-glucoside, Thr24, Thr26, His41, Cys44, Ser46, Asn142, Gly143, Ser144, Cys145, His164, Glu166, Pro168, Gln189, Thr190, Ile213, Arg217, Asp248, Gln256, Thr257, Gln299, Cys300, Ser301, Gly302 for 5R83-Demethyloleoeuropein, Thr24, Thr25, Thr26, His41, Cys44, Thr45, Ser46, Asn119, Phe140, Asn142, Gly143, Ser144, Cys145, Glu166, His172, Gln189 for 5R83-Oleuropein aglycone) have interacted through hydrogen bonds with the ligands Luteolin-7-O-glucoside, Demethyloleoeuropein, and Oleuropein aglycone respectively. The amino acids (mainlyThr31, Val73, Pro96, Tyr118, Pro122, Met165, Pro168, Leu262 for 5R83-Luteolin-7-O-glucoside, Leu27, Leu50, Cys145, Pro168, Ile213, Cys300, Val303 for 5R83-Demethyloleoeuropein, Leu27, Met49, Cys145, Met165, Leu167 for5R83-Oleuropein aglycone) were involved in hydrophobic interactions with the ligands Luteolin-7-O-glucoside, Demethyloleoeuropein, and Oleuropein aglycone respectively. The residues Ser10, Asn72 for 5R83-Luteolin-7-O-glucoside, Asn142, Glu166 for 5R83-Demethyloleoeuropein, and Phe140, Asn142, Glu166for 5R83-Oleuropein aglycone showed some ionic interactions with the ligands. In summary, for 5R83-Luteolin-7-O-glucoside, 5R83-Demethyloleoeuropein, and 5R83-Oleuropein aglycone, many hydrogen bonds were established between Thr24, Thr26, Asn142, Gly143, Ser144, Glu189, and

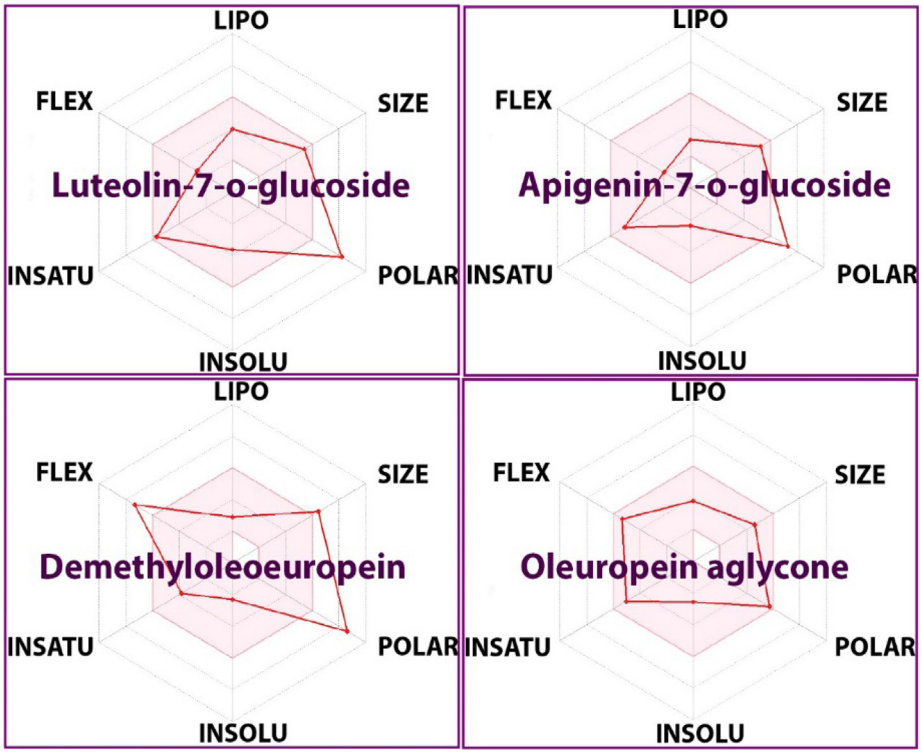

Fig. 9 *In-silico* pharmacokinetic assessment of investigated compounds. LPO lipophilicity, POLAR polarity, INSOLU solubility, FLEX flexibility and INSAT saturation.

the binding pocket- 2 of M^{pro} were observed, indicating that these amino acid residues interact strongly with the ligands in all possible directions. Similarly, with several studies, we found His41 and Cys145 (catalytic dyad) strongly interact with both Demethyloleoeuropein and Oleuropein aglycon [37–40]. Additionally, for 5R83-Luteolin-7-O-glucoside 5R83-Demethyloleoeuropein and 5R83-Oleuropein aglycone water bridges were existed in parallel along with hydrogen bonding in the majority of residues (Fig. 8).

All of the ligand properties fluctuate through the beginning or the intermediate simulation periods but progressively return to equilibrium by the end of the simulation, indicating that the four phenolic compounds or ligands are stable at the active site of the protein M^{pro}. Finally, the Oleuropein aglycon is more stable and can be explored for new drug design.

3.5. Calculation for prime (MMGBSA)

The MMGBSA binding energies obtained for all simulated complexes concerning time (last 20 ns) were in the following order: Oleuropein aglycone < Luteolin-7-o-glucoside < Apige nin-7-oglucoside < Demethyloleoeuropein, Oleuropein aglycone they had the most binding energy and, as a result, the least binding affinity to the main protease M^{pro}. Out of the four selected phenolic compounds, Oleuropein aglycone displayed the lowest total binding free energy. Among all the interactions, the contribution of the Coulomb energy (Coulomb), and the Van der Waals energy were more remarkable than other items of binding free energy (Table 3) [41].

3.6. Pharmacokinetics and drug-likeness predictions

The *in-silico* pharmacokinetic and drug-likeness properties of the four phenolic compounds and the Absorption and Toxicity of investigated phenolic compounds from leaves of *Phillyrea angustifolia* L are mentioned in (Table 4 and Fig. 9). The SwissADME prediction revealed that the TPSA value of investigated phenolic compounds from leaves of *Phillyrea angustifolia* L is closely correlated with the number of hydrogen-bond donors and acceptors.

As a result, the total polar surface area (TPSA) values of the investigated compounds are ranged from 122.52 to 212.67 $Å^2$. The Apigenin 7-glucoside (4), Luteolin-7-O-glucoside (4) and Oleuropein aglycone (8) have several rotatable bonds, which are fewer than 10 except Demethyloleoeuropein, this indicates that those compounds are conformationally stable [42,43]. The physicochemical properties of Apigenin 7-glucoside and Oleuropein aglycone only obeyed the Lipinski rule of 5 with no violation, and they had a moderate bioavailability score that implies good oral bioavailability for all investigated compounds. The rest of the lead likeness and synthetic accessibility implies that four phenolic compounds are not apt for optimization and can be easily synthesized. Moreover, the synthetic accessibility value of these phenolic compounds (except for Demethyloleoeuropein) was less than 6, which indicated their feasibility to synthesis. Furthermore, Consensus Log Po/w (the average of all five lipophilicity predictions) of four phenolic compounds is less than 5, which is within the acceptable range; their drug

score and drug-likeness indicated that these phenolic compounds are more properly to be used as drugs.

Drug development has become more and more difficult in the current situation due to poor pharmacokinetic and safety profiles of new chemical entities (NCE) [44]. Several computational approaches could help us predictions of drug-likeness activity and potential toxicity of novel compounds in the initial phases of drug discovery. The toxicity profiles of selected phenolic compounds showed less toxic probability. From our obtained results, it may be concluded that the studied phenolic chemicals do not cause AMES toxicity (*Salmonella typhimurium* reverse mutation assay), hepatotoxicity, or skin sensitization. Human colon adenocarcinoma-2 (Caco2) cell line permeability and human intestinal absorption (HIA) are important parameters to determine the overall bioavailability of a drug. All four phenolic compounds displayed comparatively low $Caco_2$ permeability potential ($< 0.61 \times 10–6$ cm/s) and could be absorbed via the human intestine, the degree of the percentage of human intestinal absorption increases in the following order Oleuropein aglycone < Apigenin-7-gluco side < Luteolin-7-O-glucoside < Demethyloleoeuropein. High toxicity was detected for all the investigated phenolic compounds in *Tetrahymena pyriformis* with an over the value of 0.285 (log μg/L) [45]. Finally, the Max tolerated dose (human) values for all phenolic compounds range from 4.63 to 6.12.

4. Conclusion

The interactions of four phenolic compounds (Luteolin-7-O-glucoside, Apigenin-7-O-glucoside, Demethyl-oleuropein, and Oleuropein aglycone) from *Phillyrea angustifolia* leaves with the SARS-CoV-2 M^{pro} has revealed strong binding contacts in the two active pockets of a target protein of SARS-CoV-2 M^{pro} with the lowest binding energies. These interactions were further investigated in MD simulation studies of this manuscript to validate the ligand-receptor contacts. The timeline interaction profile of MD simulations during the entire 100 ns showed that Demethyloleoeuropein and Oleuropein aglycon directly interacted with active site residues His41 and Cys145 (catalytic dyad) and other amino acids of the binding pocket of M^{pro}. According to QSAR, pharmacokinetics, and drug-likeness property studies, it has been suggested that Oleuropein aglycone (D) may be the best inhibitor of SARS-CoV-2 for the design and development of new drugs. Therefore, it is highly recommended to process *in vivo*, *in vitro*, and clinical studies to examine the possible potentials of these phenolic compounds in the fight against COVID-19.

Declaration of Competing Interest

The authors declare that they have no known competing financial interests or personal relationships that could have appeared to influence the work reported in this paper.

Acknowledgements

The authors acknowledge the financial support through Researchers Supporting Project number (RSP-2021/147), King Saud University, Riyadh, Saudi Arabia. This work was supported by Shandong University postdoctoral fellowship to Mohnad Abdalla, the excellent doctoral scholarship award by the Chinese Scholarship Council to Mohamed Sharaf.

References

[1] Z. Allam, *The First 50 days of COVID-19: A Detailed Chronological Timeline and Extensive Review of Literature Documenting the Pandemic*. Surveying the Covid-19 Pandemic and its Implications, 2020: p. 1-7.
[2] D. Cucinotta, M. Vanelli, WHO declares COVID-19 a pandemic, Acta Bio-Med.: Atenei Parmensis 91 (1) (2020) 157–160.
[3] T.P. Velavan, C.G. Meyer, The COVID-19 epidemic, Trop. Med. Int. Health 25 (3) (2020) 278–280.
[4] S. Ullrich, C. Nitsche, The SARS-CoV-2 main protease as drug target, Bioorg. Med. Chem. Lett. 30 (17) (2020).
[5] M. Abdalla, R.K. Mohapatra, A.K. Sarangi, P.K. Mohapatra, W.A. Eltayb, M. Alam, A.A. El-Arabey, M. Azam, S.I. Al-Resayes, V. Seidel, K. Dhama, In silico studies on phytochemicals to combat the emerging COVID-19 infection, J. Saudi Chem. Soc. 25 (12) (2021).
[6] M. Abdalla et al, Molecular dynamic study of SARS-CoV-2 with various S protein mutations and their effect on thermodynamic properties, Comput. Biol. Med. 141 (2022) 105025.
[7] K. Mou, et al., *Emerging mutations in envelope protein of SARS-CoV-2 and their effect on thermodynamic properties*. Inf. Med. Unlocked, 25 (2021) 100675.
[8] A. Citarella, A. Scala, A. Piperno, N. Micale, SARS-CoV-2 Mpro: A potential target for peptidomimetics and small-molecule inhibitors, Biomolecules 11 (4) (2021) 607.
[9] R. Banerjee, L. Perera, L.M.V. Tillekeratne, Potential SARS-CoV-2 main protease inhibitors, Drug Discov. Today 26 (3) (2021) 804–816.
[10] R.S. Joshi et al, Discovery of potential multi-target-directed ligands by targeting host-specific SARS-CoV-2 structurally conserved main protease, J. Biomol. Struct. Dyn. 39 (9) (2021) 3099–3114.
[11] D.V. Parums, Editorial: Current status of oral antiviral drug treatments for SARS-CoV-2 infection in non-hospitalized patients, Med. Sci. 28 (2022).
[12] M.A.A. Ibrahim, A.H.M. Abdelrahman, L.A. Jaragh-Alhadad, M.A.M. Atia, O.R. Alzahrani, M.N. Ahmed, M.S. Moustafa, M.E.S. Soliman, A.M. Shawky, P.W. Paré, M.-E. Hegazy, P.A. Sidhom, Exploring toxins for hunting SARS-CoV-2 main protease inhibitors: molecular docking, molecular dynamics, pharmacokinetic properties, and reactome study, Pharmaceuticals 15 (2) (2022) 153.
[13] Y.-P. Hung, J.-C. Lee, C.-W. Chiu, C.-C. Lee, P.-J. Tsai, I.-L. Hsu, W.-C. Ko, Oral nirmatrelvir/ritonavir therapy for COVID-19: the dawn in the dark?, Antibiotics 11 (2) (2022) 220
[14] R. Abiri, H. Abdul-Hamid, O. Sytar, R. Abiri, E. Bezerra de Almeida, S.K. Sharma, V.P. Bulgakov, R.R.J. Arroo, S. Malik, A brief overview of potential treatments for viral diseases using natural plant compounds: the case of SARS-Cov, Molecules (Basel, Switzerland) 26 (13) (2021) 3868.
[15] B. Nazim, T. Houari, B. Ismail, Ethnobotanical survey of some plants used in Tessala Region, Algeria, Curr. Perspect. Med. Aromat. Plants (CUPMAP) 3 (1) (2020) 25–30.
[16] S. Faisal, S.L. Badshah, B. Kubra, M. Sharaf, A.-H. Emwas, M. Jaremko, M. Abdalla, Computational study of SARS-CoV-2 RNA dependent RNA polymerase allosteric site inhibition, Molecules 27 (1) (2021) 223.
[17] A. Romani, A. Baldi, N. Mulinacci, F.F. Vincieri, M. Tattini, Extraction and identification procedures of polyphenolic compounds and carbohydrates in phillyrea (Phillyrea

angustifolia L.) leaves, Chromatographia 42 (9-10) (1996) 571–577.
[18] S. Kim, P.A. Thiessen, E.E. Bolton, J. Chen, G. Fu, A. Gindulyte, L. Han, J. He, S. He, B.A. Shoemaker, J. Wang, B. Yu, J. Zhang, S.H. Bryant, PubChem substance and compound databases, Nucleic Acids Res. 44 (D1) (2016) D1202–D1213.
[19] D. Fearon, et al., *PanDDA analysis of COVID-19 main protease against the DSI-poised Fragment Library*. PDB ID: 5R82, 2020.
[20] A. Douangamath, D. Fearon, P. Gehrtz, T. Krojer, P. Lukacik, C.D. Owen, E. Resnick, C. Strain-Damerell, A. Aimon, P. Ábrányi-Balogh, J. Brandão-Neto, A. Carbery, G. Davison, A. Dias, T.D. Downes, L. Dunnett, M. Fairhead, J.D. Firth, S.P. Jones, A. Keeley, G.M. Keserü, H.F. Klein, M.P. Martin, M.E. M. Noble, P. O'Brien, A. Powell, R.N. Reddi, R. Skyner, M. Snee, M.J. Waring, C. Wild, N. London, F. von Delft, M.A. Walsh, Crystallographic and electrophilic fragment screening of the SARS-CoV-2 main protease, Nat. Commun. 11 (1) (2020).
[21] C. Sarkar, et al., *Ebselen suitably interacts with the potential SARS-CoV-2 targets: an in-silico approach*. J. Biomol. Struct. Dynam., (2021) 1-16.
[22] F. Ghasemi, A. Mehridehnavi, A. Pérez-Garrido, H. Pérez-Sánchez, Neural network and deep-learning algorithms used in QSAR studies: merits and drawbacks, Drug Discov. Today 23 (10) (2018) 1784–1790.
[23] K. Roy, S. Kar, R.N. Das, A Primer on QSAR/QSPR Modeling: Fundamental Concepts. 2015: Springer.
[24] S. Kwon, H. Bae, J. Jo, S. Yoon, Comprehensive ensemble in QSAR prediction for drug discovery, BMC Bioinf. 20 (1) (2019).
[25] B.J. Neves et al, QSAR-based virtual screening: advances and applications in drug discovery, Front. Pharmacol. 9 (2018) 1275.
[26] A. Daina, O. Michielin, V. Zoete, SwissADME: a free web tool to evaluate pharmacokinetics, drug-likeness and medicinal chemistry friendliness of small molecules, Sci. Rep. 7 (1) (2017) 1–13.
[27] F. Cheng, W. Li, Y. Zhou, J. Shen, Z. Wu, G. Liu, P.W. Lee, Y. Tang, admetSAR: a comprehensive source and free tool for assessment of chemical ADMET properties, J. Chem. Inf. Model. 52 (11) (2012) 3099–3105.
[28] G.M. Benhander, A.A.A. Abdusalam, Identification of potential inhibitors of SARS-CoV-2 main protease from Allium roseum L. molecular docking study, Chemistry Africa 5 (1) (2022) 57–67.
[29] R.K. Mohapatra, L. Perekhoda, M. Azam, M. Suleiman, A.K. Sarangi, A. Semenets, L. Pintilie, S.I. Al-Resayes, Computational investigations of three main drugs and their comparison with synthesized compounds as potent inhibitors of SARS-CoV-2 main protease (Mpro): DFT, QSAR, molecular docking, and in silico toxicity analysis, J. King Saud Univ.-Sci. 33 (2) (2021).
[30] A. Kumer, M.N. Sarker, P. Sunanda, The theoretical investigation of HOMO, LUMO, thermophysical properties and QSAR study of some aromatic carboxylic acids using HyperChem programming, Int. J. Chem. Technol. 3 (1) (2019) 26–37.
[31] F. Limanaqi, C.L. Busceti, F. Biagioni, G. Lazzeri, M. Forte, S. Schiavon, S. Sciarretta, G. Frati, F. Fornai, Cell clearing systems as targets of polyphenols in viral infections: Potential implications for COVID-19 pathogenesis, Antioxidants 9 (11) (2020) 1105.
[32] J.A.C. Nascimento Junior, A.M. Santos, L.J. Quintans-Júnior, C.I.B. Walker, L.P. Borges, M.R. Serafini, MERS and SARS-CoV-2 (COVID-19) treatment: a patent review, Expert Opin. Ther. Pat. 30 (8) (2020) 567–579.
[33] E. Pitsillou et al, Interaction of small molecules with the SARS-CoV-2 main protease in silico and in vitro validation of potential lead compounds using an enzyme-linked immunosorbent assay, Comput. Biol. Chem. 89 (2020) 107408.
[34] J. Koča, Z. Kříž, P.H.J. Carlsen, Computer study of conformational flexibility of 20 common amino acids, J. Mol. Struct. (Thoechem) 306 (2–3) (1994) 157–164.
[35] H.U. Rashid, N. Ahmad, M. Abdalla, K. Khan, M.A.U. Martines, S. Shabana, Molecular docking and dynamic simulations of Cefixime, Etoposide and Nebrodenside A against the pathogenic proteins of SARS-CoV-2, J. Mol. Struct. 1247 (2022) 131296.
[36] M.J. Yunta, It is important to compute intramolecular hydrogen bonding in drug design, Am. J. Model. Optim 5 (1) (2017) 24–57.
[37] A. Garg, et al., *Virtual screening of natural products inspired in-house library to discover potential lead molecules against the SARS-CoV-2 main protease*. J. Biomol. Struct. Dynam., (2022) 1-13.
[38] A.K. Ray et al, Repurposing of FDA-approved drugs as potential inhibitors of the SARS-CoV-2 main protease: Molecular insights into improved therapeutic discovery, Comput. Biol. Med. 142 (2022) 105183.
[39] E. Fornasier, M.L. Macchia, G. Giachin, A. Sosic, M. Pavan, M. Sturlese, C. Salata, S. Moro, B. Gatto, M. Bellanda, R. Battistutta, A new inactive conformation of SARS-CoV-2 main protease, Acta Crystallogr. Sect., D: Struct. Biol. 78 (3) (2022) 363–378.
[40] J.H. Zothantluanga, et al., Computational Investigations for Identification of Bioactive Molecules from Baccaurea ramiflora and Bergenia ciliata as Inhibitors of SARS-CoV-2 Mpro 1 29.
[41] C.J. Ononamadu et al, In silico identification and study of potential anti-mosquito juvenile hormone binding protein (MJHBP) compounds as candidates for dengue virus - Vector insecticides, Biochem. Biophys. Rep. 28 (2021) 101178.
[42] C.A. Lipinski, Drug-like properties and the causes of poor solubility and poor permeability, J. Pharmacol. Toxicol. Methods 44 (1) (2000) 235–249.
[43] C.A. Lipinski, Lead-and drug-like compounds: the rule-of-five revolution, Drug Discov. Today: Technol. 1 (4) (2004) 337–341.
[44] J. Chen et al, Drug discovery and drug marketing with the critical roles of modern administration, Am. J. Transl. Res. 10 (12) (2018) 4302–4312.
[45] D.E.V. Pires, T.L. Blundell, D.B. Ascher, pkCSM: predicting small-molecule pharmacokinetic and toxicity properties using graph-based signatures, J. Med. Chem. 58 (9) (2015) 4066–4072.